

Magnetocaloric properties of Nd-doped Gd_5Si_4 microparticles and nanopowders

Kaiyang Zhang(张凯扬), Huanhuan Wang(王欢欢), Ying Wang(王颖), and Tao Wang(王涛)

Citation: Chin. Phys. B, 2024, 33 (**11**): 117502. DOI: 10.1088/1674-1056/ad6de7
Journal homepage: http://cpb.iphy.ac.cn; http://iopscience.iop.org/cpb

What follows is a list of articles you may be interested in

Magnetic and magnetocaloric effect of $Er_{20}Ho_{20}Dy_{20}Cu_{20}Ni_{20}$ high-entropy metallic glass

Shi-Lin Yu(于世霖), Lu Tian(田路), Jun-Feng Wang(王俊峰), Xin-Guo Zhao(赵新国), Da Li(李达), Zhao-Jun Mo(莫兆军), and Bing Li(李昺)
Chin. Phys. B, 2024, 33 (**5**): 057502. DOI: 10.1088/1674-1056/ad1a94

Mechanical and magnetocaloric adjustable properties of Fe_3O_4/PET deformed nanoparticle film

Fengguo Fan(范凤国) and Lintong Duan(段林彤)
Chin. Phys. B, 2024, 33 (**3**): 037502. DOI: 10.1088/1674-1056/acf280

Magnetocaloric properties of phenolic resin bonded $La(Fe,Si)_{13}$-based plates and its use in a hybrid magnetic refrigerator

Shao-Shan Xu(徐少山), Qi Fu(付琪), Yi-Fan Zhou(周益帆), Ling Peng(彭铃), Xin-Qiang Gao(高新强), Zhen-Xing Li(李振兴), Mao-Qiong Gong(公茂琼), Xue-Qiang Dong(董学强), and Jun Shen(沈俊)
Chin. Phys. B, 2023, 32 (**2**): 027502. DOI: 10.1088/1674-1056/ac9fbf

Magnetic and magnetocaloric effect in a stuffed honeycomb polycrystalline antiferromagnet $GdInO_3$

Yao-Dong Wu(吴耀东), Wei-Wei Duan(段薇薇), Qiu-Yue Li(李秋月), Yong-Liang Qin(秦永亮),Zhen-Fa Zi(訾振发), and Jin Tang(汤进)
Chin. Phys. B, 2022, 31 (**6**): 067501. DOI: 10.1088/1674-1056/ac43a1

Comprehensive performance of a ball-milled $La_{0.5}Pr_{0.5}Fe_{11.4}Si_{1.6}B_{0.2}H_y$/Al magnetocaloric composite

Jiao-Hong Huang(黄焦宏), Ying-De Zhang(张英德), Nai-Kun Sun(孙乃坤), Yang Zhang(张扬), Xin-Guo Zhao(赵新国), and Zhi-Dong Zhang(张志东)
Chin. Phys. B, 2022, 31 (**4**): 047503. DOI: 10.1088/1674-1056/ac280b

---

Magnetocaloric properties of Nd-doped Gd_5Si_4 microparticles and nanopowders

Kaiyang Zhang(张凯扬), Huanhuan Wang(王欢欢), Ying Wang(王颖)[†], and Tao Wang(王涛)[‡]

School of Physical Science and Technology, Lanzhou University, Lanzhou 730000, *China*

(Received 9 May 2024; revised manuscript received 9 August 2024; accepted manuscript online 12 August 2024)

The preparation of materials with enhanced magnetocaloric properties is crucial for magnetic refrigeration. In this study, Nd-doped Gd_5Si_4 microparticles and nanomaterials were synthesized using the reduction–diffusion method. The impact of Nd doping with varying compositions on the structure and entropy change properties of the materials was investigated. The Curie temperatures of both the micron- and nano-sized materials ranged from 190 K to 210 K, which were lower than previously reported values. Micron-sized samples doped with 1% Nd exhibited superior magnetocaloric properties, demonstrating a maximum entropy change of 4.98 $J{\cdot}kg^{-1}{\cdot}K^{-1}$ at 5 T, with an entropy change exceeding 4 $J{\cdot}kg^{-1}{\cdot}K^{-1}$ over a wide temperature range of approximately 70 K. Conversely, the nanomaterials had broader entropy change peaks but lower values. All samples exhibited a second-order phase transition, as confirmed by the Arrott plots.

Keywords: magnetocaloric, Gd_5Si_4, Nd doping, reduction–diffusion method

PACS: 75.30.Sg **DOI:** 10.1088/1674-1056/ad6de7

1. Introduction

High-performance magnetocaloric materials for magnetic refrigeration offer potential solutions to the environmental impact caused by current refrigeration technology. However, challenges remain for magnetic refrigeration materials, including limited selection, narrow temperature intervals for entropy changes, small entropy changes, low saturation magnetization strengths, and inappropriate Curie temperatures. Their capabilities do not fulfill the requirements for technological advancement.[1–5] Thus, the development of magnetic materials with high magnetocaloric transformation efficiencies, wide entropy change intervals, suitable Curie temperatures, high purities, and good reproducibility remains a challenge.[6–10] Alloyed materials with first-order magnetic phase transitions, such as $Gd_5(Si_xGe_{1-x})_4$, $LaFe_{11.4}Si_{1.6}$, $MnFeP_{0.45}As_{0.55}$, and $MnAs_{1-x}Sb_x$, often exhibit significant magnetic entropy transition peaks. However, thermal and magnetic hystereses limit the cooling effects of these materials and restrict their operation to a narrow temperature range. For the $Gd_5(Si_xGe_{1-x})_4$ system, the phase transition becomes a second-order transition, with the ferromagnetic to paramagnetic transition occurring for x values greater than 0.5, thereby avoiding thermal hysteresis.[11,12] Consequently, this study focused on the Gd_5Si_4 system, which is known for its relatively large entropy change.[13–18] The half-full 4f orbitals of the rare earth element Gd result in a large theoretical magnetic moment, leading to an enhanced magnetocaloric effect.[19–23] Metal ion substitution is a common method for enhancing the magnetic properties of $Gd_5(Si_xGe_{1-x})_4$ materials.[24–30] Doping with Nd can induce charge transfer of 5d electrons from Gd to Nd, thereby enhancing the magnetization response of the substituted compounds to low magnetic fields.[26] Consequently, this study utilized Nd doping to improve the magnetocaloric properties of Gd_5Si_4 alloy. The reduction–diffusion method, commonly employed in the production of permanent magnets, was adopted to explore novel preparation processes for Gd_5Si_4 alloys. Additionally, the samples were ball-milled into nanocrystals to leverage the benefits of nanosizing, including a broader temperature range for entropy change.[31]

2. Experiments

$(Gd_{1-x}Nd_x)_5Si_4$ ($x = 0.01$–0.025) alloy samples were created using the reduction–diffusion method. High-purity Gd_2O_3 powder (> 99.99% by mass), calcium particles (> 99% by mass), silicon powder (> 99.99% by mass), and Nd_2O_3 powder (> 99.99% by mass) were purchased from GRINM Advanced Materials Co., Ltd. (China) and were mixed in proportions outlined in Table 1, where the proportion of Si exceeded the chemical ratio by 35%.

Table 1. Proportions of raw materials.

Doped Nd ratio (%)	Gd_2O_3 (g)	Ca (g)	Si (g)	Nd_2O_3 (g)
1.0	17.944	9.018	3.033	0.168
1.5	17.853	9.018	3.033	0.252
2.0	17.762	9.018	3.033	0.337
2.5	17.672	9.018	3.033	0.421

The raw materials were mixed in a blending tank to achieve full homogeneity and then compressed into disks at 40 MPa. Subsequently, the disks were placed in a vacuum atmosphere furnace, where they underwent a reaction at 850 °C

[†]Corresponding author. E-mail: yingw@lzu.edu.cn
[‡]Corresponding author. E-mail: wtao@lzu.edu.cn

© 2024 Chinese Physical Society and IOP Publishing Ltd

for 7 h, followed by a 1.5 h hold at 1200 °C, and finally cooled to room temperature naturally. The crushed samples were sieved through a 100-mesh sieve to obtain micron-sized powders. Pure Nd-doped Gd_5Si_4 micron-sized powders were obtained by washing the samples with acid, water, ethanol, and acetone. The samples were labeled N1, N1.5, N2, and N2.5, respectively. The micron-scale materials were subjected to 10 h planetary ball milling with water as the milling medium to ensure a thorough breakdown and to obtain nanosized crystal particles. The ball-milled samples were named N1M, N1.5M, N2M, and N2.5M, respectively.

The crystal structures of the magnetic powders were determined using x-ray diffraction (XRD) with a Cu $K\alpha$ source (Rigaku Ultima IV). The surfaces and compositions of the samples were analyzed using scanning electron microscopy (SEM; TESCAN MIRA 3) and energy dispersive spectrometry (EDS). The proportion of Ca was determined using inductively coupled plasma-optical emission spectrometry (ICP-OES; Plasma Quant PQ9000). The morphologies and crystal structures of the ball-milled samples were characterized using transmission electron microscopy (TEM; FEI Talos F200 C). The field cooling (FC) curves (100 Oe; 10–340 K; 3 K·min^{-1}) for the magnetization of the samples and the isothermal M–H curves (50 kOe; 150–250 K) were measured using a superconducting quantum interference device (SQUID, Quantum Design) to determine the Curie temperatures (T_C), saturation magnetization (M_s), and isothermal entropy changes ($-\Delta S$) of the samples.[25–27]

3. Results and discussion

3.1. Phase analyses

Figure 1(a) presents the XRD patterns of the N1, N1.5, N2, and N2.5 samples compared with the standard JCPDS card (No. 79-1642). No impurity peaks were observed in the samples doped with different amounts of Nd, and all diffraction peaks were sharp and intense, indicating the high crystallinity of the prepared samples.

The XRD patterns of the N1M, N1.5M, N2M, and N2.5M samples are illustrated in Fig. 1(b). GdSi impurity peaks were detected in the post-ball-milled samples, with Gd_5Si_3 impurities precipitating from the N1.5M sample. Ball milling was shown to cause significant disruption to the crystal structure of the samples due to the high-energy impact. However, the main phase of Gd_5Si_4 was still maintained in the samples. The broadening of the diffraction peaks can be attributed to various factors, such as the reduction in grain size,[18,28,30] lattice strain, and lattice defects. Assuming that the reduction in grain size was the main factor, the nanoparticle sizes were estimated using the Scherrer formula

$$D = \frac{K\gamma}{B\cos\theta}, \tag{1}$$

where K is the Scherrer constant ($K = 0.89$ if B is the full width at half maximum of the diffraction peak), D is the average thickness of the grain perpendicular to the crystal plane direction, B is the measured sample diffraction peak width at half height (radian), θ is the Bragg angle (angle), and γ is the x-ray wavelength (generally 1.54056 Å). The grain sizes are presented in Table 2, indicating successful nanosizing of the samples through ball milling.

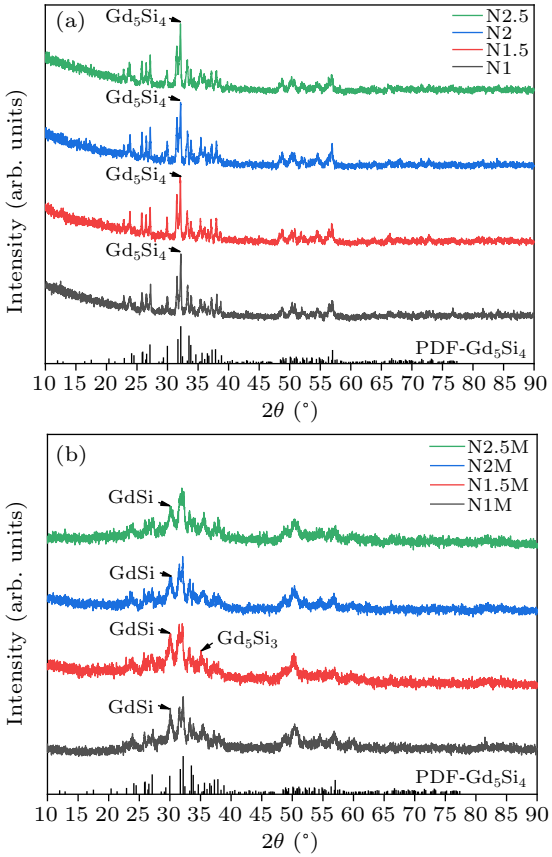


Fig. 1. (a) XRD patterns of N1, N1.5, N2, and N2.5; (b) XRD patterns of N1M, N1.5M, N2M, and N2.5M.

Table 2. Grain sizes of the ball-milled samples estimated using the Scherrer formula.

Sample	B (°)	2θ (°)	D (nm)
N1M	0.264	32.144	35
N1.5M	0.204	32.071	45
N2M	0.240	32.002	39
N2.5M	0.181	32.173	51

3.2. Morphological analyses

Figure 2 shows the SEM images and EDS elemental analyses of the N2.5 sample. The images revealed that the particles ranged in size from 1 μm to 5 μm, with most exhibiting porous structures and a few displaying layered structures, making them prone to breakage.

The EDS analysis indicated that the Gd and Si proportions generally met the requirements, whereas the Nd proportion was not accurately determined using this method. Additionally, the washed samples still contained Ca (∼ 8% based

on the EDS measurement; ∼ 15% based on the ICP-OES measurement) owing to difficulties in completely removing Ca from the crystal lattice during the experimental preparation process. The EDS scan image revealed a uniform distribution of Ca without any signs of aggregation, suggesting that Ca was incorporated into the lattice rather than existing as CaO. When Ca atoms were substituted into the lattice, they altered the lattice dimensions, which was evident in the XRD pattern by a shift in the diffraction peaks without the emergence of new impurity phases. For the N1 sample, the main peak (231) of the Gd_5Si_4 phase was observed at $2\theta = 32.144°$, slightly deviating from the standard JCPDS card value of 32.228°.

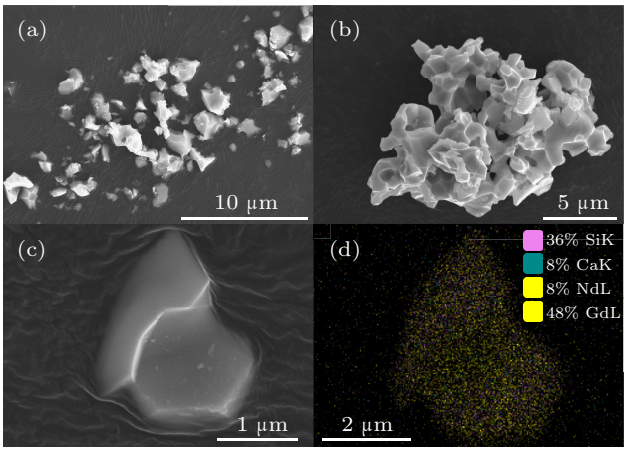


Fig. 2. (a)–(c) SEM images of the N2.5 sample; (d) EDS scan and composition ratio of (c).

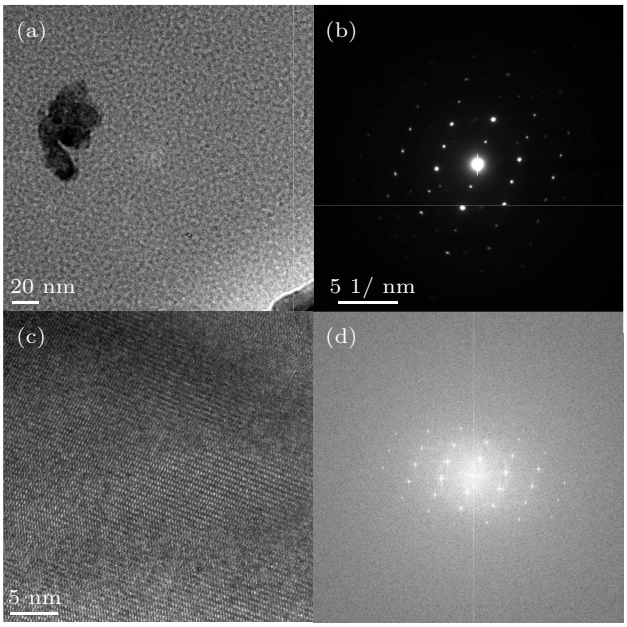


Fig. 3. (a) TEM images, (b) EDP image, and (c) HRTEM image of the N2M sample. (d) Fast Fourier transform image of (c).

The samples obtained through ball milling were examined using TEM and HRTEM to assess their level of crystallization. As illustrated in Fig. 3, the individual particles were relatively small, measuring approximately 40 nm, which was consistent with the result calculated using the Scherrer formula. Both the EDP and HRTEM images demonstrated a high degree of crystallization in the sample.

3.3. Phase transition characteristics

Figure 4 shows the FC curves of the samples. The phase transition temperatures of the four samples occurred within a wide range of 170–230 K, leading to a significant decrease in magnetic properties. The FC curves of N1M, N1.5M, N2M, and N2.5M indicated noticeable reductions in magnetization after ball milling, particularly in the samples with higher Nd contents.

With increased Nd doping, the lattice stability decreased, resulting in more severe damage to the crystal structures after ball milling. The GdSi and Gd_5Si_3 impurity phases that emerged after ball milling were antiferromagnetic with Néel temperatures of 55 K.[32,33] They contributed negligibly to the magnetic moment under an external magnetic field of 100 Oe. Nevertheless, the phase transition range remained relatively consistent, ranging from 170 K to 230 K. The Curie temperatures of the samples were determined by identifying the peak positions of the $\mathrm{d}M/\mathrm{d}T$ curves, and they are listed in Table 3. These Curie temperatures, approximately 200 K, were significantly lower than the reported values for Gd_5Si_4 bulk (∼ 336 K[34]) and micropowders (∼ 320 K[18]). This deviation could be attributed to the presence of nonmagnetic Ca ions in the lattice, which disrupted the RKKY exchange interactions among the magnetic Gd ions.

Table 3. Curie temperatures of the samples.

Sample	Curie temperature (K)
N1	202
N1M	209
N1.5	194
N1.5M	210
N2	201
N2M	204
N2.5	202
N2.5M	203

It can be observed in Fig. 4 that the temperature range exhibiting the most significant changes in the magnetic properties of the samples was 150–250 K. Subsequently, the isothermal magnetization curves were measured, and the entropy changes in this range were calculated.

3.4. Analyses of the entropy changes

The N1, N1M, N2, and N2M samples were chosen for isothermal magnetization testing on account of their more stable magnetic performance and fewer impurities observed in the XRD patterns.

Figures 5(a) and 5(c) demonstrate that the magnetization of the N1 sample reached approximately 130 emu·g^{-1} at a

temperature of 150 K under a magnetic field of 5 T. Following 10 h of ball milling, although the magnetism of the N1M sample decreased, it still reached 60 emu·g^{-1} under the same conditions, indicating that the magnetization of the ball-milled sample remained favorable. As shown in Figs. 5(b) and 5(d), the magnetization of the N2 sample was approximately 115 emu·g^{-1} at a temperature of 150 K under a magnetic field of 5 T. In contrast, the magnetization decreased with increased Nd doping, which was consistent with the FC curves. The magnetization of the N2M sample decreased to nearly 20 emu·g^{-1} under the same conditions, demonstrating both inferior magnetism and stability.

Based on a series of isothermal magnetization curves, the $-\Delta S$ values of the samples were calculated using Maxwell's relation[15,35]

$$\Delta S(T,H) = S(T,H) - S(T,0) = \mu_0 \int_0^H \left(\frac{\partial M}{\partial T}\right)_H \mathrm{d}H. \quad (2)$$

In practice, a numerical integration is performed using the following formula:

$$\Delta S(T,H) = \mu_0 \sum_i \frac{M_i - M_{i+1}}{T_i - T_{i+1}} \delta H. \quad (3)$$

Plots of $-\Delta S$ versus temperature ($-\Delta S$ vs. T) were obtained for the samples with an applied magnetic field of 0–5 T. The results are shown in Fig. 6.[15,25–27]

Figure 6 presents the $-\Delta S$ vs. T curves and 3D renderings of the N1 and N2 samples. The curves exhibited similar changes at different magnetic field strengths, showing a wide temperature range for high $-\Delta S$. The $-\Delta S$ values of both samples initially increased and then decreased with increasing temperature under the same applied magnetic field. The N1 sample reached a maximum $-\Delta S$ value of 4.98 J·kg^{-1}·K^{-1} at approximately 207 K, whereas the N2 sample reached a maximum value of 4.11 J·kg^{-1}·K^{-1} at a lower temperature of approximately 194 K, which was attributed to the increase in the Nd component. Compared to bulk Gd_5Si_4,[15] the N1 sample exhibited a slightly lower peak value of $-\Delta S$ than the 6.94 J·kg^{-1}·K^{-1} of the bulk material, although the peak of the $-\Delta S$ was broader. The temperature at which the $-\Delta S$ remained above 4 J·kg^{-1}·K^{-1} was approximately 70 K for the N1 sample and approximately 60 K for the bulk material. The broadening of the $-\Delta S$ peaks may have been attributed to the presence of Ca ions in the samples, leading to inhomogeneous defects and pinning centers that resulted in variations in the phase transition temperatures. Notably, the $-\Delta S$ values of these samples were comparable to those of Gd_5Si_4 powders produced by the melting method,[18] although the $-\Delta S$ peaks were even broader.

The $-\Delta S$ vs. T curves and 3D renderings of the ball-milled N1M and N2M samples are presented in Fig. 7. The figure indicates that the magnetic entropy peaks of the samples were broader than those of the unmilled samples, whereas the $-\Delta S$ values were generally lower. The N1M and N2M samples exhibited maximum $-\Delta S$ values of approximately 200 K, with values of 1.93 J·kg^{-1}·K^{-1} and 0.51 J·kg^{-1}·K^{-1}, respectively. The $-\Delta S$ value of the N2M sample was slightly greater in the low-temperature region under a high magnetic field. These observations, in conjunction with the FC curves, were attributed to the presence of superparamagnetic nanoparticles in the N2M sample.

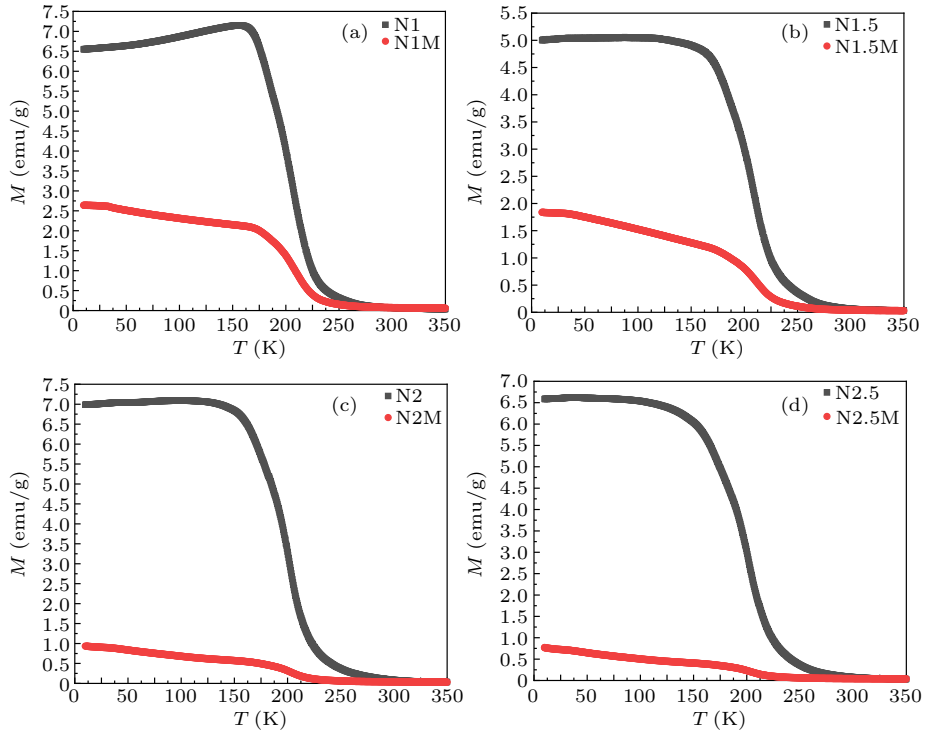


Fig. 4. FC curves of the samples with applied magnetic fields of 100 Oe. (a) N1 and N1M, (b) N1.5 and N1.5M, (c) N2 and N2M, and (d) N2.5 and N2.5M.

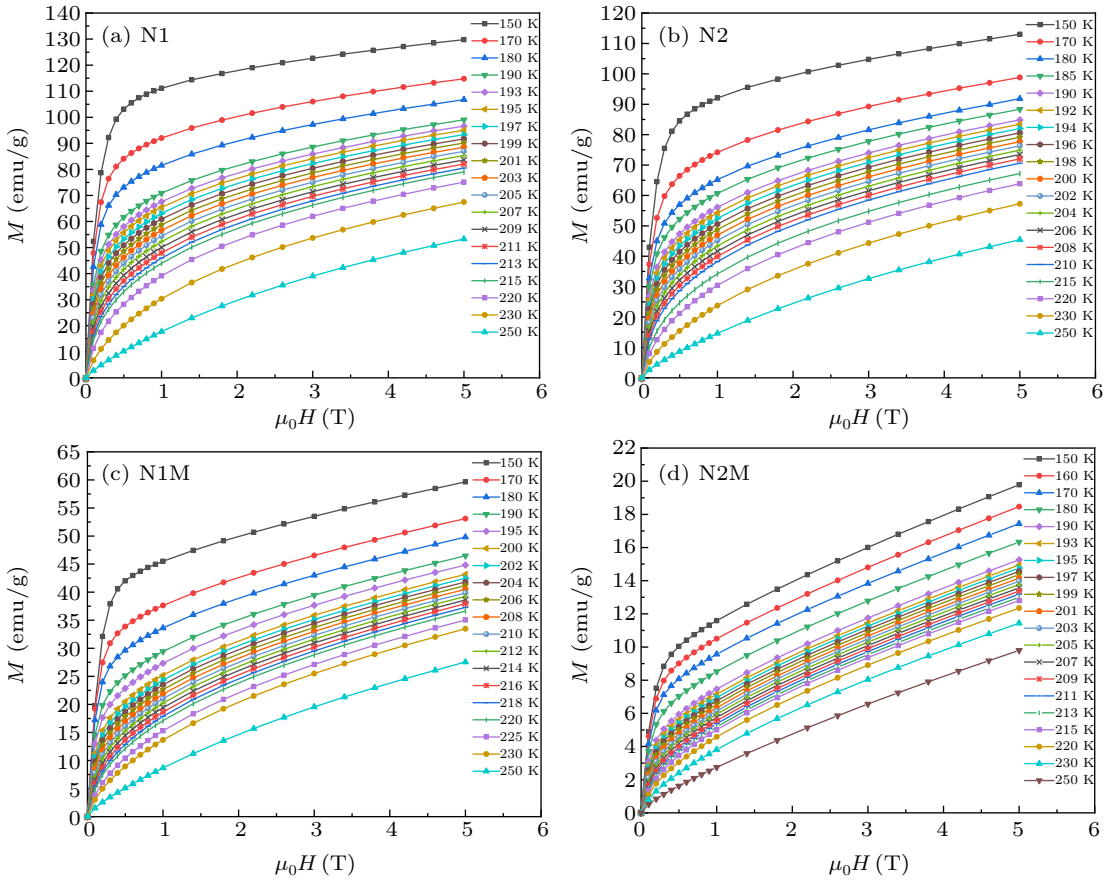


Fig. 5. The *M*–*H* curves of the (a) N1, (b) N2, (c) N1M, and (d) N2M samples at different temperatures.

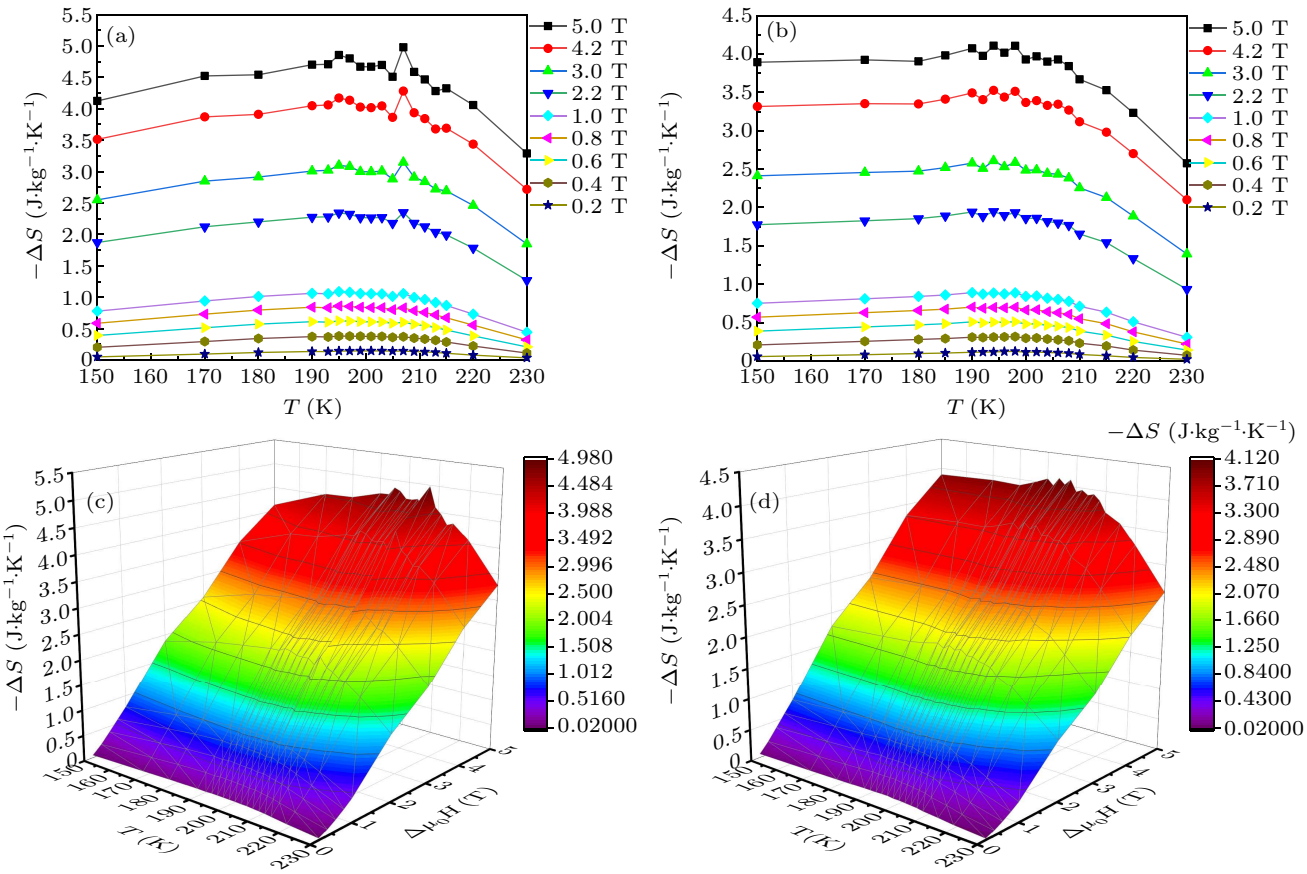


Fig. 6. The $-\Delta S$ versus T plots and 3D renderings for the (a), (c) N1 and (b), (d) N2 samples.

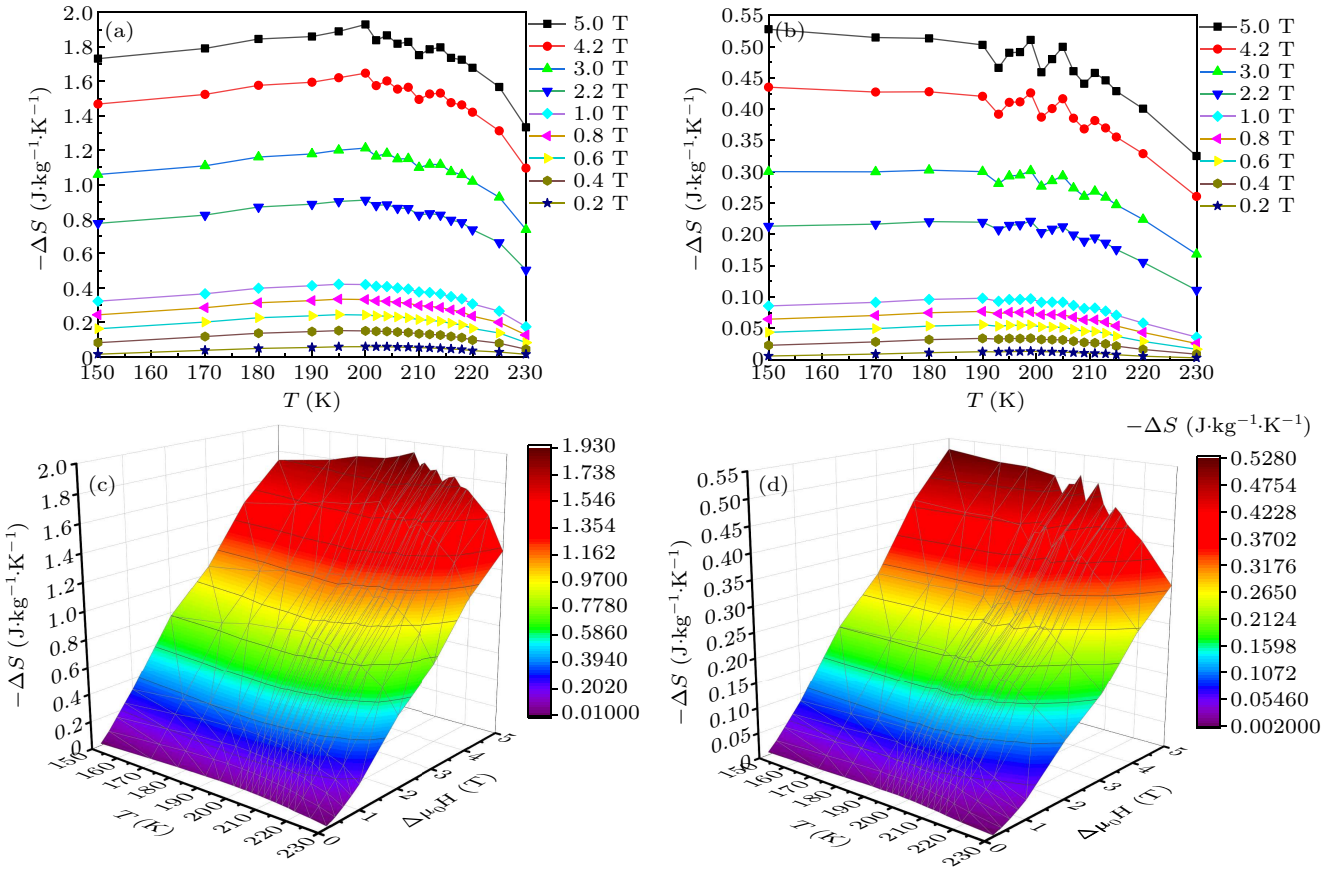


Fig. 7. The $-\Delta S$ versus T plots and 3D renderings of the (a), (c) N1M and (b), (d) N2M samples.

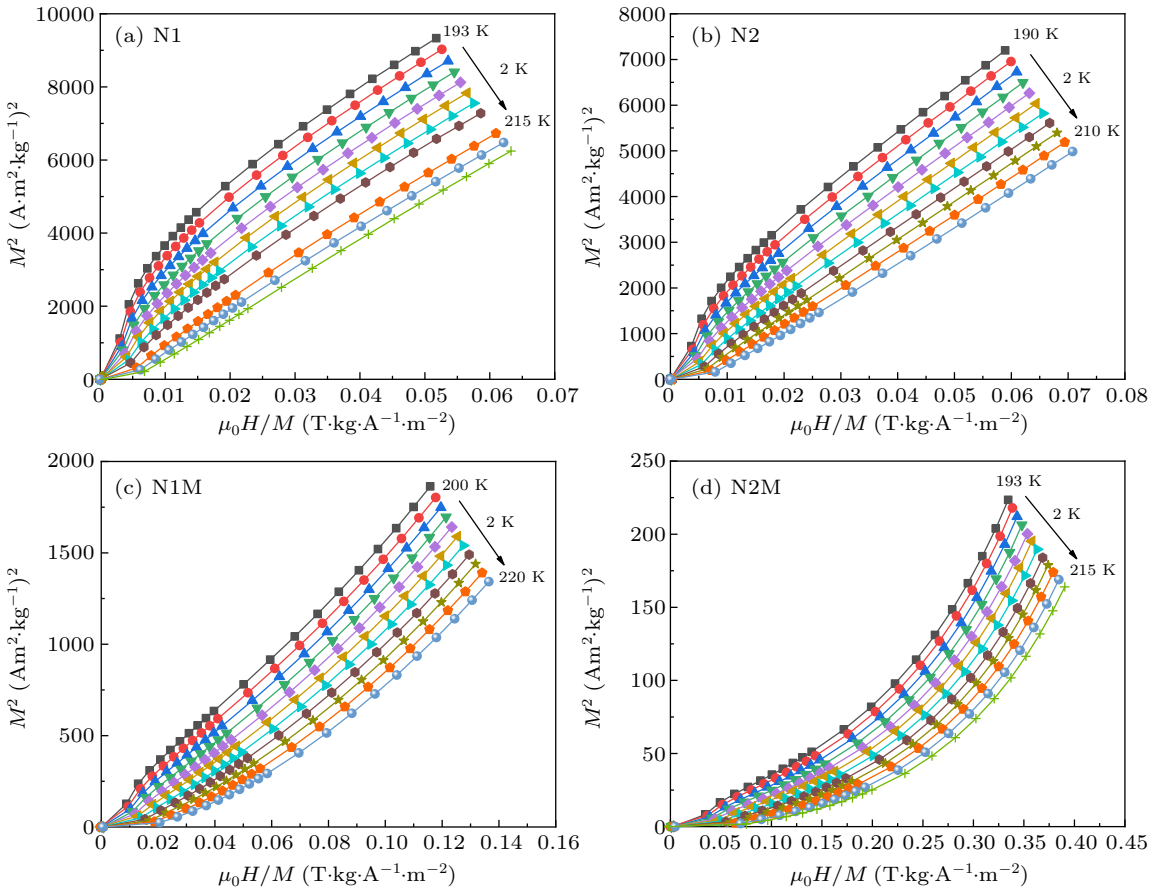


Fig. 8. Arrott plots M^2 vs. $\mu_0 H/M$ for (a) N1, (b) N2, (c) N1M, and (d) N2M.

3.5. Analysis of the phase transition

To analyze whether the phase transition type of the samples was affected by Nd doping and residual Ca atoms, Arrott plots[36] were created (Fig. 8): M^2 versus B/M calculated from the isothermal magnetization $M(H)$ curves.

For all samples, the Arrott plots exhibited positive slopes. The upper sections of the Arrott plots for the N1 and N2 samples demonstrated the expected linear dependence for a second-order phase transition,[37] suggesting that the phase transition type of the samples was unaffected by the presence of Nd and Ca atoms. The nonlinear deviations at low fields may be attributed to inhomogeneities.[38] The Arrott plots of the N1M and N2M samples displayed similar trends at low and medium fields; however, they showed nonlinear deviations at high fields, particularly for the N2M sample, indicating the presence of higher-order terms or varying coefficients of the M^2 term in the Landau free energy expansion. These deviations may have been caused by the emergence of impurity phases and superparamagnetic nanoparticles following ball milling.

4. Conclusion and perspectives

Nd-doped Gd_5Si_4 micromaterials and nanomaterials with high magnetothermal conversion efficiencies, wide entropy change intervals, and high phase purities were prepared using the reduction–diffusion method. The Curie temperatures of these micromaterials and nanomaterials were significantly reduced and generally ranged between 190 K and 210 K. The micromaterials doped with 1% Nd exhibited superior magnetocaloric properties. The magnetization was 129.79 emu·g^{-1} at 150 K and 5 T. The maximum value of $-\Delta S$ reached approximately 4.98 J·kg^{-1}·K^{-1} at approximately 207 K under 5 T and exceeded 4 J·kg^{-1}·K^{-1} in the temperature range of approximately 70 K (150–220 K). The corresponding nanomaterials exhibited broader entropy change peaks, albeit with lower values. According to the Arrott plots, all samples exhibited second-order phase transitions. These results demonstrate the potential of Nd-doped Gd_5Si_4 materials prepared via the reduction–diffusion method as magnetic refrigeration materials. Furthermore, the results suggest that the proposed method may be a promising approach for the synthesis of Gd_5Si_4 series alloys.

Acknowledgment

Project supported by the Natural Science Foundation of Gansu Province (Grant No. 22JR5RA404).

References

[1] Gschneidner K A, Pecharsky V K and Tsokol A O 2005 *Rep. Prog. Phys.* **68** 1479
[2] Gschneidner K A and Pecharsky V K 2000 *Annu. Rev. Mater. Res.* **30** 387
[3] Pecharsky V K and Gschneidner K A 1999 *J. Magn. Magn. Mater.* **200** 44
[4] Hao J Z, Hu F X, Yu Z B, Shen F R, Zhou H B, Gao Y H, Qiao K M, Li J, Zhang C, Liang W H, Wang J, He J, Sun J R and Shen B G 2020 *Chin. Phys. B* **29** 047504
[5] Brown G V 1976 *J. Appl. Phys.* **47** 3673
[6] Franco V, Blázquez J S, Ingale B and Conde A 2012 *Annu. Rev. Mater. Res.* **42** 305
[7] Oesterreicher H and Parker F T 1984 *J. Appl. Phys.* **55** 4334
[8] Shen B G, Sun J R, Hu F X, Zhang H W and Cheng Z H 2009 *Adv. Mater.* **21** 4545
[9] Tegus O, Brück E, Buschow K H J and de Boer F R 2002 *Nature* **415** 150
[10] Balli M, Jandl S, Fournier P and Kedous-Lebouc A 2017 *Appl. Phys. Rev.* **4** 021305
[11] Banerjee B K 1964 *Phys. Lett.* **12** 16
[12] Dan'kov S Y, Tishin A M, Pecharsky V K and Gschneidner K A 1998 *Phys. Rev. B* **57** 3478
[13] Holtzberg F, Gambino R J and McGuire T R 1967 *J. Phys. Chem. Solids* **28** 2283
[14] Pecharsky V K and Gschneidner Jr. K A 2001 *Adv. Mater.* **13** 683
[15] Hu P Q, Zhang Z M, Zhang F X, Guan W Z, Wang D H and Du Y W 2022 *Curr. Appl. Phys.* **34** 95
[16] Morellon L, Algarabel P A, Ibarra M R, Blasco J, García-Landa B, Arnold Z and Albertini F 1998 *Phys. Rev. B* **58** R14721
[17] Pecharsky V K and Gschneidner K A 1997 *J. Alloys Compd.* **260** 98
[18] Harstad S M, El-Gendy A A, Gupta S, Pecharsky V K and Hadimani R L 2019 *JOM* **71** 3159
[19] Pecharsky V K and Gschneidner Jr. K A 1997 *Phys. Rev. Lett.* **78** 4494
[20] Choe W, Pecharsky V K, Pecharsky A O, Gschneidner K A, Young V G and Miller G J 2000 *Phys. Rev. Lett.* **84** 4617
[21] Pecharsky A O, Gschneidner K A and Pecharsky V K 2003 *J. Appl. Phys.* **93** 4722
[22] Tang B Z, Liu X P, Li D M, Yu P and Xia L 2020 *Chin. Phys. B* **29** 056401
[23] Levin E M, Pecharsky V K and Gschneidner K A 1999 *Phys. Rev. B* **60** 7993
[24] Provenzano V, Shapiro A J and Shull R D 2004 *Nature* **429** 853
[25] Uthaman B and Raama Varma M 2015 *Mater. Sci. Forum* **830–831** 501
[26] Kou R H, Gao J, Ren Y, Sanyal B, Bhandary S, Heald S M, Fisher B and Sun C J 2018 *AIP Adv.* **8** 125219
[27] Nikitin S, Smirnov A, Bogdanov A and Ovchenkova I 2018 *EPJ Web of Conferences* **185** 05006
[28] Pavan Kumar N, Prabahar K, Raj Kumar D M and Manivel Raja M 2019 *J. Supercond. Novel Magn.* **32** 319
[29] Zhang T B, Chen Y G, Tang Y B, Du H J, Ren T and Tu M J 2007 *J. Alloys Compd.* **433** 18
[30] Paixão L S, Rangel G, Usuda E O, Imamura W, Tedesco J C G, Patiño J C, Gomes A M, Alves C S and Carvalho A M G 2020 *J. Magn. Magn. Mater.* **493** 165693
[31] Nauman M, Alnasir M H, Hamayun M A, Wang Y X, Shatruk M and Manzoor S 2020 *RSC Adv.* **10** 28383
[32] Canepa F, Cirafici S and Napoletano M 2002 *J. Alloys Compd.* **335** L1
[33] Tung L D, Lees M R, Balakrishnan G and Paul D M 2005 *Phys. Rev. B* **71** 144410
[34] Altounian Z and Liu X B 2007 *J. Appl. Phys.* **101** 09
[35] Landers J, Salamon S, Keune W, Gruner M E, Krautz M, Zhao J, Hu M Y, Toellner T S, Alp E E, Gutfleisch O and Wende H 2018 *Phys. Rev. B* **98** 024417
[36] Arrott A and Noakes J E 1967 *Phys. Rev. Lett.* **19** 786
[37] Aharoni A 1986 *J. Magn. Magn. Mater.* **58** 297
[38] Duc N H, Kim Anh D T and Brommer P E 2002 *Physica B* **319** 1